11th Int. Symp. on Turb. Shear Flow, Vol. 3, pp. 26.1–26.6, Grenoble, 1997 (Eq. 3 corrected)

Large Eddy Simulation: A Dynamic One-Equation Subgrid Model for Three-Dimensional Recirculating Flow

Lars Davidson
Dep. of Thermo and Fluid Dynamics, Chalmers University of Technology
S-412 96 Gothenburg, Sweden

ABSTRACT

Standard dynamic subgrid models have numerical stability problems. The remedy is to average in some homogeneous flow direction(s) or to introduce some artificial clipping. Thus this type of models do not seem to be applicable to real three-dimensional flow without introducing *ad hoc* user modifications. In the present study a new one-equation subgrid model is presented which reduces the need of this type of user-modifications. The present model is a modification of the model presented in Ref. [5]. The model is applied to recirculating flow in an enclosure.

INTRODUCTION

Germano *et al.* [10, 11] propose a dynamic subgrid model in which the constant in the Smagorinsky model is not arbitrarily chosen (or optimized), but where it is computed. The dynamic models which have been developed have problems with negative values of the C-coefficient. When a negative C occurs it is believed to represent *backscatter*, i.e. spectral flow of energy from subgrid scales to resolved scales. This means that the production term in the transport equation for subgrid kinetic energy $P_{k_{sgs}} = -\tau^a_{ij}\bar{u}_{i,j}$ becomes negative, and feeds energy back to the resolved scales. The problem is that negative diffusion (negative C) causes numerical problems. These can be handled as long as the total (i.e. viscous plus turbulent) diffusion is positive. However, large negative, turbulent diffusion remains a problem. It is not only negative values on C that causes numerical problems. It exhibits very strong gradients and "fluctuates wildly" [23]. In a ventilated enclosure, for example, the author has found that C varies typically in the range ± 4 which should be compared with a standard value of the Smagorinsky constant $C_S^2 = 0.01$. In the literature [23, 19, 24, 20, 2, 22, 6, 17, 18] it has been found that in order to achieve numerical stability present dynamic subgrid models require either that there exist a homogeneous flow direction or that the dynamic coefficient is clipped at some arbitrary limit in an *ad hoc* manner. Thus the model does not seem to be applicable to real three-dimensional flows where no homogeneous flow direction exists.

An attempt to improve this restriction was presented by Ghosal *et al.* [13, 12] where they try to optimize the equation for C globally, but still with the constraint that $C > 0$. This optimization leads to an integral equation (Fredholm's integral equation of the second kind) which is very expensive to solve numerically. They report that it increases the CPU time by 50% [1].

In the present work a new one-equation dynamic subgrid model is applied to recirculating flow in an enclosure. It is an modification of the model presented in Ref. [5].

THE ONE-EQUATION MODEL

If we follow Germano [9] and introduce *generalized* central moments the transport equation for the subgrid kinetic energy k_{sgs} reads [4]

$$\frac{\partial k_{sgs}}{\partial t} + (\bar{u}_j k_{sgs})_{,j} = -\mathcal{T}_f(u_i,u_j)\bar{u}_{i,j} - \left\{\frac{1}{2}\mathcal{T}_f(u_j,u_i,u_i) + \mathcal{T}_f(u_j,p/rho)\right\}_{,j} + \nu(k_{sgs})_{,jj} - \nu\mathcal{T}_f(u_{i,j},u_{i,j}). \quad (1)$$

The dynamic coefficient C in the production term

$$\begin{aligned} P_{k_{sgs}} &= -\tau^a_{ij}\bar{u}_{i,j} \\ \tau^a_{ij} &\equiv \mathcal{T}_f(u_i,u_j) = -2C\Delta k_{sgs}^{\frac{1}{2}}\bar{S}_{ij} \end{aligned} \quad (2)$$

is computed in a similar way as in the standard dynamic model [10, 11, 13, 12], i.e.

$$\begin{aligned} C &= -\frac{\mathcal{L}_{ij}M_{ij}}{2M_{ij}M_{ij}};\ \mathcal{L}_{ij} = \widehat{\bar{u}_i\bar{u}_j} - \widehat{\bar{u}}_i\widehat{\bar{u}}_j \\ K &= \widehat{k_{sgs}} + \frac{1}{2}\mathcal{L}_{ii} \\ M_{ij} &= \widehat{\Delta}K^{\frac{1}{2}}\widehat{\bar{S}}_{ij} - \Delta\,\widehat{k_{sgs}^{\frac{1}{2}}\bar{S}_{ij}} \end{aligned} \quad (3)$$

where $\mathcal{L}_{ij}$ denotes the *dynamic* Leonard stresses, and where $K \equiv \frac{1}{2}T_{ii}$ is the subgrid kinetic energy on the test level [13, 12, 4]. The diffusion constant can also be computed dynamically as in Refs. [13, 12]. In the present study

the standard gradient hypothesis is used with the turbulent Prandtl number set to one. The dissipation term $\varepsilon_{k_{sgs}}$ is estimated as

$$\varepsilon_{k_{sgs}} \equiv \nu \mathcal{T}_f(u_{i,j}, u_{i,j}) = C_* \frac{k_{sgs}^{\frac{3}{2}}}{\Delta}. \quad (4)$$

In order to estimate C_* attention is turned to the transport equation for K. The equations for k_{sgs} and K read in symbolic form

$$C_{k_{sgs}} - D_{k_{sgs}} = P_{k_{sgs}} - C_* \frac{k_{sgs}^{\frac{3}{2}}}{\Delta} \quad (5)$$

$$C_K - D_K = P_K - C_* \frac{K^{\frac{3}{2}}}{\widehat{\Delta}}. \quad (6)$$

where C and D on the left-hand sides denote convection and diffusion, respectively. Apply the test filter to Eq. 5. In Ref. [5] an ASM-like expression was used, which was found to have an undesired positive feedback feature, which made it necessary to restrict the variations in the C_*-coefficient. Here we use a modified relation. The transport of k_{sgs} is set proportional to that of K so that

$$\widehat{P}_{k_{sgs}} - \frac{1}{\Delta}\widehat{C_* k_{sgs}^{\frac{3}{2}}} = \left(P_K - C_* \frac{K^{\frac{3}{2}}}{\widehat{\Delta}} \right), \quad (7)$$

and we obtain

$$C_*^{n+1} = \left(P_K - \widehat{P}_{k_{sgs}} + \frac{1}{\Delta}\widehat{C_*^n k_{sgs}^{\frac{3}{2}}} \right) \frac{\widehat{\Delta}}{K^{\frac{3}{2}}}. \quad (8)$$

The dissipation cannot be negative which requires that we limit C_* to positive values, i.e. $C_* \geq 0$. In Eq. 8 C_* is kept inside the filtering process. Following Piomelli [20] the dynamic coefficient under the filter is taken at the old time-step.

To ensure numerical stability a *constant* value of C in space ($\langle C \rangle_{xyz}$) is used in the momentum equations, which is determined by requiring that the production in the whole computational domain should remain the same, i.e.

$$\langle 2C\Delta k_{sgs}^{\frac{1}{2}} \bar{S}_{ij} \bar{S}_{ij} \rangle_{xyz} = 2\langle C \rangle_{xyz} \langle \Delta k_{sgs}^{\frac{1}{2}} \bar{S}_{ij} \bar{S}_{ij} \rangle_{xyz} \quad (9)$$

The idea is to include all local dynamic information through the source terms of the transport equation for k_{sgs}. This is probably physically more sound since large local variations of C appear only in the source term, and the effect of the large fluctuations in the dynamic coefficients will be smoothed out in a natural way. This means that the need to restrict or limit the dynamic coefficient is reduced or may not be necessary altogether. However, *if* we have to restrict the dynamic coefficients in the k_{sgs} equation this does not affect the results as much as if the coefficient in the original dynamic model is restricted. The reason is that in the one-equation model the coefficients affect the stresses only in an indirect way (the source terms are part of a transport equation) whereas in the original dynamic model the dynamic C-coefficient is linearly proportional to the stresses. It is extremely important to use subgrid models which are numerically stable and where the need to introduce *ad hoc* modification is limited as far as possible, if we want to develop turbulence models applicable to general flow situations.

The spatial variation of C is included via the production term in the modelled k_{sgs} equation. In this way backscatter is taken into account in an indirect way. Although it is not fed *directly* back to the resolved flow, it influences the resolved flow via the kinetic subgrid energy. A negative production reduces k_{sgs} and this effect influences the neighborhood through convection and diffusion of k_{sgs}.

The new model can be summarized as follows:

1. The equation for the kinetic subgrid energy is solved (Eq. 1);

2. The production term (see Eq. 2) is computed using the *local* dynamic coefficient (Eq. 3) without any averaging or restrictions;

3. The turbulent Prandtl number in the diffusion term is set to one;

4. The local dynamic coefficient in front of the dissipation term is computed from Eq. 8;

5. The subgrid stresses in the momentum equation are computed using a *homogeneous* values $\langle C \rangle_{xyz}$ of the dynamic coefficient determined from Eq. 9; $\langle C \rangle_{xyz}$ is also used in the diffusion term in the k_{sgs} equation.

6. The boundary condition for k_{sgs} is zero at all boundaries.

The boundary conditions for k_{sgs} does not seem to affect the results much, and the reason is that the equation is dominated by its source terms, production and dissipation (see Fig. 8b).

Some limits on C_* *are* used. It is not allowed to go negative (this occurs in approximately 25% of the nodes). A limit is also used to prevent C_* from growing too large. Presently an arbitrary value of 10 is used; this limit is reached in approximately 0.3% of the nodes. It is presently not clear if this limit is needed at all. Note that the present formulation for C_* in Eq. 8 is considerably better than that used in Ref. [5].

THE NUMERICAL METHOD

An implicit, two-step time-advancement methods is used. When the filtered Navier-Stokes equation for $\bar{u}_i$

$$\frac{\partial \bar{u}_i}{\partial t} + \frac{\partial}{\partial x_j}(\bar{u}_i \bar{u}_j) = -\frac{1}{\rho}\frac{\partial \bar{p}}{\partial x_i} + \nu \frac{\partial^2 \bar{u}_i}{\partial x_j \partial x_j} - \frac{\partial \tau_{ij}}{\partial x_j} \quad (10)$$

is discretized it can be written

$$\bar{u}_i^{n+1} = \bar{u}_i^n + \Delta t H\left(u_i^n, u_i^{n+1}\right) - \frac{1}{\rho}\alpha \Delta t \frac{\partial p^{n+1}}{\partial x_i} - \frac{1}{\rho}(1-\alpha)\Delta t \frac{\partial p^n}{\partial x_i} \quad (11)$$

where $H\left(u_i^n, u^{n+1}\right)$ includes convection and the viscous and subgrid stresses, and $\alpha = 0.5$ (Crank-Nicolson). Equation 11 is solved which gives $\bar{u}_i^{n+1}$ which does not satisfy continuity. An intermediate velocity field is computed by subtracting the implicit part of the pressure gradient, and the resulting Poisson equation is solved employing an efficient multigrid method. For more details, see Refs. [5, 16, 8, 7].

RESULTS

A steady computation is first carried out using the CALC-BFC code and the $k-\varepsilon$ model [3]. These results are used as initial start fields in the LES calculations. The predictions are compared with Laser-Doppler measurements of Restivo [21] (also available in Ref. [15]). The geometry is given by (see Fig. 1):

$$L/H = 3,\ W/H = 1,\ h/H = 0.056,\ t/H = 0.16$$
$$Re = \frac{U_{in} h}{\nu} = 5000.$$

where W is the extent of the domain in the z direction. We have used $H = 3$ m, $U_{in} = 0.455$ m/s, and air of 20°C. Inlet boundary conditions are set as

$$\bar{u}_{in} = U_{in} + rnd \cdot u_{rms,exp} \quad (12)$$
$$\bar{v}_{in} = rnd \cdot u_{rms,exp},\ \bar{w}_{in} = rnd \cdot u_{rms,exp}$$

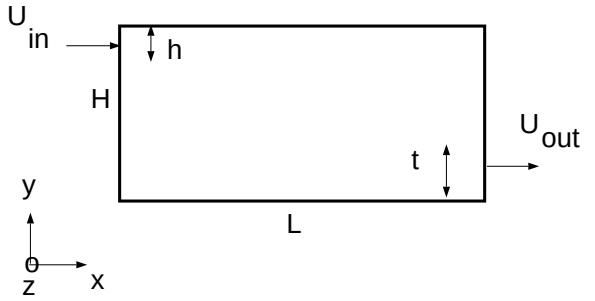

Figure 1: Ventilated enclosure.

Homogeneous inlet profiles are used for all variables. Note that the random function rnd is called at different times for $\bar{u}_{in}$, $\bar{v}_{in}$ and $\bar{w}_{in}$, which means that the fluctuations are not correlated so that $(\overline{\bar{u}\bar{v}})_{in} = (\overline{\bar{u}\bar{w}})_{in} = (\overline{\bar{v}\bar{w}})_{in} = 0$.

At the outlet the exit velocity is computed from global continuity and it is taken as constant over the outlet. Zero gradient is set for the remaining variables.

At all six walls traditional wall functions [3] are used if $y^+ > 11$. Along the ceiling these are never used as the boundary layer is well resolved ($y^+ < 3$ for the first node).

A $96 \times 64 \times 64$ grid has been used. A hyperbolic tangent function is used in x and z direction, whereas geometric stretching is used in the y direction. At the position $x/H = 2$ (see Fig. 6) 17 nodes are located inside the velocity maximum, $y_{1/2}$ corresponds to $y/H = 0.89$, and for the near-wall node $y^+ \simeq 2$. For more details, see Ref. [5]. The number of time steps used in each calculation is typically 40000 using a maximum CFL number of approximately two. This corresponds to approximately 2200 seconds. The streamwise average of the peak velocity in the wall jet along the ceiling is close to $U_{av} = 0.5U_{in}$ ($= 0.228$ m/s). Thus the time it takes for a fluid particle to move from the inlet to the opposite wall can be estimated as $L/U_{av} \simeq 40$ seconds, which means that $2200/40 = 55$ characteristic time units (L/U_{av}) are covered in a simulation. Averaging has been performed during the last 19 000 time steps. Tests presented in [3] show that this is more than enough. Unless otherwise stated all results presented have been obtained with the new dynamic one-equation model.

In Fig. 2 the time averaged $\bar{u}$ velocities are compared with experiments, and as can seen the agreement is good. The predicted peak velocity in the wall jet is in good agreement with experiments, much better than for the one-equation model presented in Ref. [5]. The original dynamic model [10, 11, 3] is compared with the new dynamic one-equation model. As can be seen the one-equation model performs better.

In Fig. 3 instantaneous velocity vector plots are shown. Looking at the wall jet in side view (Fig. 3a) we see the characteristic wavy pattern. This accounts for the entrainment process between the wall jet and its surrounding. If we are used to Reynolds Averaged Navier-Stokes (RANS) we can easily misinterpret the effect of turbulent (or, as in LES, subgrid) viscosity. In RANS a high turbulent viscosity gives a smeared out, diffusive velocity profile due to high diffusion of momentum in the normal direction (y). In LES it is vice versa. A high subgrid viscosity damps the resolved fluctuations which are responsible for diffusion of time-averaged momentum in the y direction and the result is a more pointed velocity profile due to reduced diffusion of momentum.

The time history of $\bar{u}$ is shown in Fig. 4. It can be seen that there is a large difference between the turbulence in the wall jet (Fig. 4a) and that in the middle of the room (Fig. 4b). The magnitude of the fluctuations in the wall jet

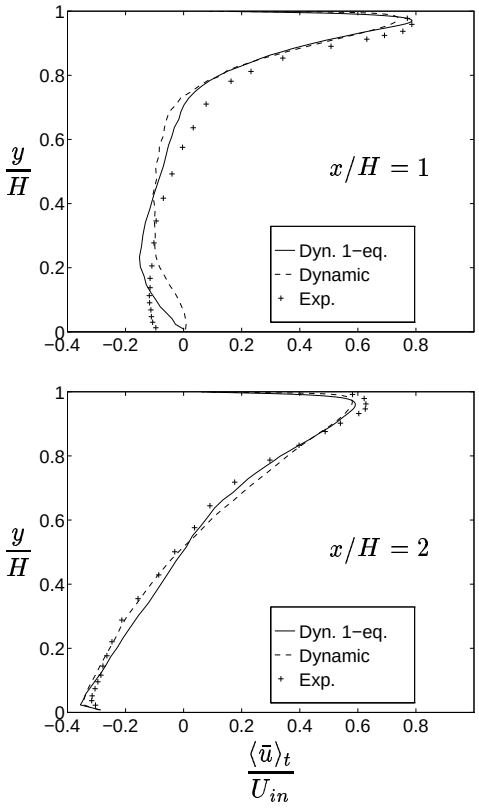

Figure 2: Time averaged velocity profiles. Symmetry plane $z/H = 0.5$. Lines: predictions; +: experimental mean velocity [21] (see also [15].

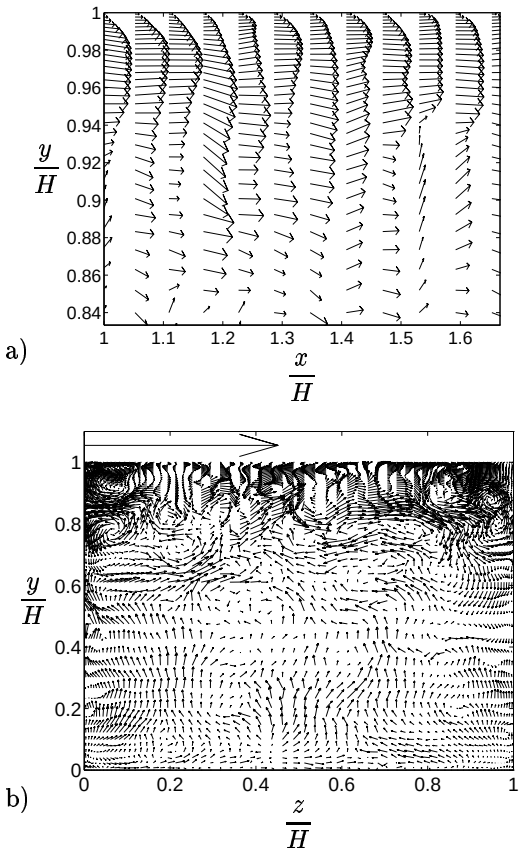

Figure 3: Vector plots. a) $z/H = 0.5$. b) $x/H = 1.5$. Reference arrow above the figure shows $U/U_{in} = 1$.

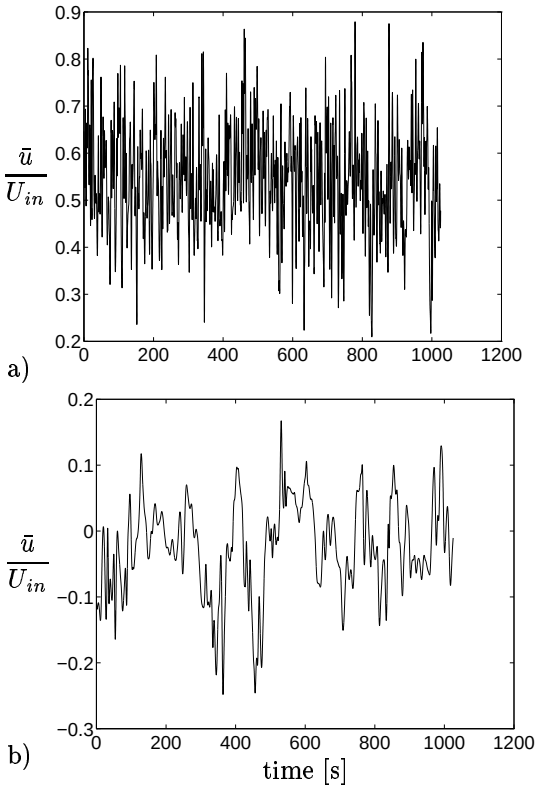

Figure 4: Time history of $\bar{u}$ at two chosen cells. $z/H = 0.5$. a) $x/H = 1.0, y/H = 0.92$. b) $x/H = 1.0, y/H = 0.5$

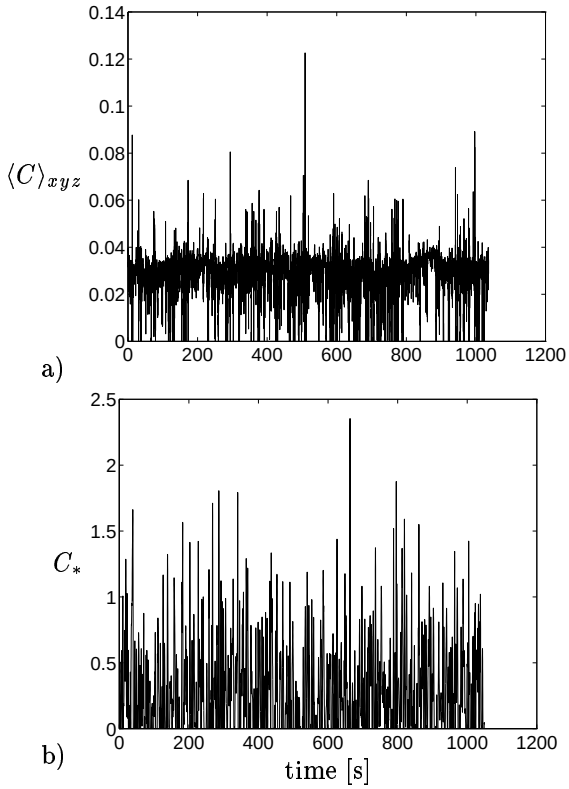

Figure 5: Time history of the dynamic coefficients. a) The dynamic coefficient $\langle C \rangle_{xyz}$. b) The dynamic coefficient C_* at one chosen cell $x/H = 2.0, y/H = 0.92, z/H = 0.5$.

is larger and there are much higher frequencies. In Fig. 4b the flow is not fully turbulent.

From the time history of the homogeneous dynamic coefficient $\langle C \rangle_{xyz}$ in Fig. 5a we find that the time averaged value is close to 0.04 which corresponds to a value of the Smagorinsky constant $C_S = 0.2$. The $\langle C \rangle_{xyz}$ coefficient sometimes (at approximately 3% of the time steps) wants to go negative, but it is clipped at zero. The C_* coefficient connected with the dissipation term in the k_{sgs} equation is presented in Fig. 5b. Its behavior is more stochastic than $\langle C \rangle_{xyz}$, because it is local. It often tends to zero, but it rarely hits the upper bound which has been set to 10. In fact, at $x/H = 2$ the C_* coefficient never becomes larger than approximately 3. Possibly the upper limit is not needed at all. Here it is clearly seen that the present model works much better than that presented in Ref. [5].

Wall jet

The flow along the ceiling is a wall jet. Thus it could be interesting to compare the predictions with wall jet data. The experiments of Karlsson *et al.* [14] have been chosen. The Reynolds number in the wall jet experiment is higher ($Re = 10000$) than in the present study.

In Fig. 6 the streamwise mean velocities, computed with the standard dynamic model and the one-equation dynamic model, are compared with experiments, and the agreement is very good. If we, however, compare the width and the maximum velocities this picture changes. The predicted wall jet spreads too much compared with experiments (see Table 1), which agrees with the comparison in Fig. 2. The peak velocity, however, agrees well with experiments, in particular for the predictions with the one-equation model. The reason for the rather poor agreement in the spreading rate could be due to insufficient grid resolution. It could also be that the subgrid models (both the dynamic and the dynamic one-equation model) give too low a subgrid viscosity. As a results this would give too large exchange of momentum in the y direction due to too little damping (by the subgrid stresses) of the resolved fluctuations.

	x/h	U_{max}/U_{in}	$d\delta_{1/2}/dx$	$y_{1/2}/h$
1-eq. model	17.9	0.786	-	2.01
1-eq. model	35.7	0.592	0.111	4.01
dyn. model	17.9	0.739	-	2.20
dyn. model	35.7	0.581	0.126	4.46
Exp.	20	0.771	-	1.88
Exp.	40	0.566	0.08	3.48

Table 1: Comparison with wall jet data [14]

The stresses in the wall jet are shown in Fig. 7. Generally, the stress levels are too low, both the normal ones and the shear stress. The stress changes sign near the wall and the location agrees well with the experimental one; the positive peak, however, is under-predicted. The dynamic Leonard stress $\mathcal{L}_{12}$ (see Eq. 3) is also included, and it is almost as large as the resolved stress. It can be seen that the subgrid stress (also included in Fig. 7) is much smaller than the resolved stress, except close to the wall. Actually, at $x/H = 2$, the time averaged subgrid turbulent viscosity is of the same order as the viscous one ($\langle \nu_{sgs} \rangle_t < 4\nu$), whereas the instantaneous value can be much higher ($\nu_{sgs,max} \simeq 26\nu$).

In Fig. 8a turbulent kinetic energies are presented. We find that the subgrid energy k_{sgs} is rather large. It is much larger than for the model presented in Ref. [5]. The reason is that the dissipation in the present study is much smaller due to a smaller C_* coefficient. The dynamic Leonard kinetic energy is a large fraction of the resolved kinetic energy. In Fig. 8b the time averaged production and dissipation term in the k_{sgs} equation are shown. As can be seen they are fairly much in balance. The spatial variation of

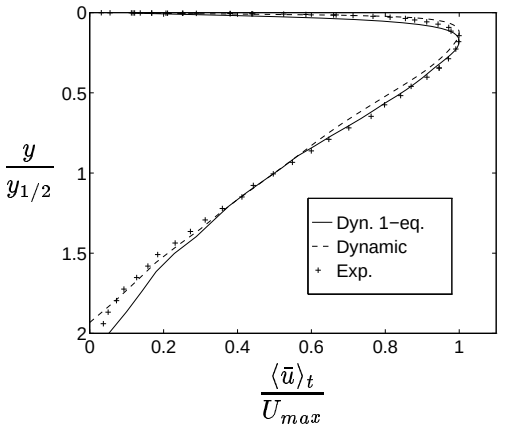

Figure 6: Time averaged velocity. $z/H = 0.5$. LES: $x/H = 2$ ($x/h = 35.7$); exp: $x/h = 40$. Solid line: 1-eq. dynamic model; dashed line: dynamic model; +: experiments [14].

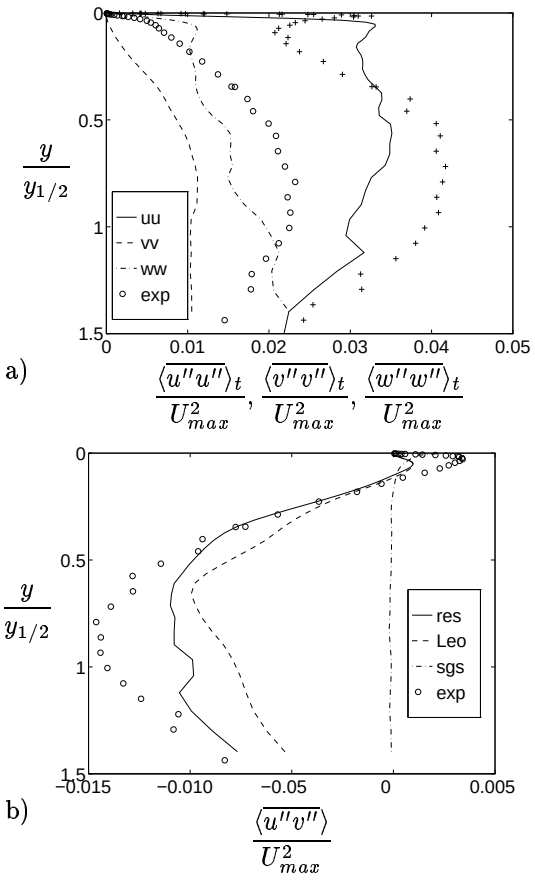

Figure 7: Resolved stresses. Symmetry plane $z/H = 0.5$. LES: $x/H = 2$ ($x/h = 35.7$); exp: $x/h = 40$. a) Solid line: $\langle u''u'' \rangle_t / U^2_{max}$; dashed line: $\langle v''v'' \rangle_t / U^2_{max}$; dash-dotted line: $\langle w''w'' \rangle_t / U^2_{max}$. +: experimental $\overline{u^2}/U^2_{max}$; ∘: experimental $\overline{v^2}/U^2_{max}$ [14]. b) Solid line: shear stress $\langle u''v'' \rangle_t / U^2_{in}$; dashed line: dynamic Leonard stress $\langle \mathcal{L}_{12} \rangle_t / U^2_{in}$; dash-dotted line: subgrid shear stress $\langle \tau_{12} \rangle_t / U^2_{in}$; ∘: experimental $\overline{uv}/U^2_{max}$[14].

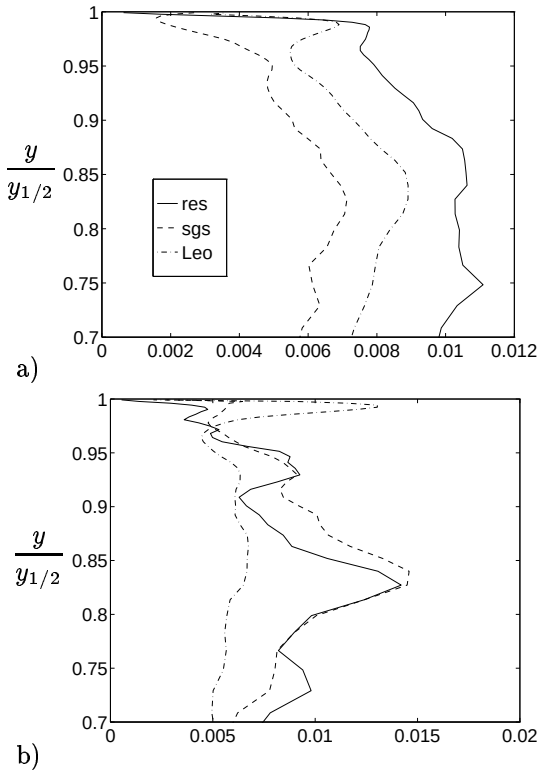

Figure 8: Symmetry plane $z/H = 0.5$. $x/H = 2$. a) Kinetic turbulent energies. Solid line: resolved turbulent kinetic energy $\frac{1}{2}\langle u_i'' u_i'' \rangle_t / U^2_{in}$; dash-dotted line: kinetic energy of dynamic Leonard stresses $\frac{1}{2}\langle \mathcal{L}_{ii} \rangle_t / U^2_{in}$; dashed line: turbulent kinetic subgrid energy $\langle k_{sgs} \rangle_t / U^2_{in}$. b) Terms in the subgrid kinetic energy equation. Solid line: production $\langle P_k \rangle_t$; dashed line: dissipation $\langle C_* k^{1.5}_{sgs}/\Delta \rangle_t$; dash-dotted line: $0.01\langle C_* \rangle_t$.

$\langle C_* \rangle_t$ at $x/H = 2$ is also included. It has values close to 0.5 except close to the wall where it attains values around 1.3.

CONCLUSIONS

A contribution towards a development of a new dynamic subgrid one-equation model has been presented. The general idea is to include dynamic information in the source terms of an equation for the turbulent kinetic subgrid energy k_{sgs} rather than directly in the momentum equations. In the momentum equation a *homogeneous* value (keeping the time dependence) of the local dynamic coefficient is used. In this way numerical stability is greatly enhanced since the large oscillation in the local dynamic coefficients enter as source terms in the k_{sgs} equation, and they are naturally smoothed out through convection and diffusion. This model naturally accounts for back-scatter since the production term in the k_{sgs} equation is permitted to go negative.

The proposed new one-equation model gives closer agreement with experimental data than the standard original dynamic model.

References

[1] Akselvoll, K., and Moin, P. Large eddy simulation of turbulent confined coannular jets and turbulent flow over a backward facing step. Report no. TF-63, Stanford University, Dept. Mech. Eng., 1995.

[2] Balaras, B., Benocci, C., and Piomelli, U. Finite-difference computations of high Reynolds number flow using the Dynamic subgrid-scale model. *Theor. and Comp. Fluid Dyn. 7* (1995), 207–216.

[3] Davidson, L. Implementation of a large eddy simulation method applied to recirculating flow in a ventilated room. Report, ISSN 1395-7953 R9611, Dep. of Building Technology and Structural Engineering, Aalborg University, 1996.[1]

[4] Davidson, L. Large eddy simulations: A note on derivation of the equations for the subgrid turbulent kinetic energies. Rept. 97/11, Dept. of Thermo and Fluid Dynamics, Chalmers University of Technology, Gothenburg, 1997.[1]

[5] Davidson, L. LES of recirculating flow without any homogeneous direction: A dynamic one-equation subgrid model. In *2nd Int. Symp. on Turbulence Heat and Mass Transfer* (Delft, 1997), pp. 481–490.[1]

[6] Davidson, L., and Nielsen, P. Large eddy simulations of the flow in a three-dimensional ventilated room. In *5th Int. Conf. on Air Distributions in Rooms, ROOMVENT'96* (Yokohama, Japan, 1996), S. Murakami, Ed., vol. 2, pp. 161–168.[1]

[7] Emvin, P. *The Full Multigrid Method Applied to Turbulent Flow in Ventilated Enclosures Using Structured and Unstructured Grids.* PhD thesis, Dep. of Thermo and Fluid Dynamics, Chalmers University of Technology, Gothenburg, 1997.

[8] Emvin, P., and Davidson, L. Development and implementation of a fast large eddy simulations method. Rept., Dept. of Thermo and Fluid Dynamics, Chalmers University of Technology, Gothenburg, 1997.

[9] Germano, M. Turbulence: the filtering approach. *Journal of Fluid Mechanics 238* (1992), 325–336.

[10] Germano, M., Piomelli, U., Moin, P., and Cabot, W. A dynamic subgrid-scale eddy viscosity model. *Phys. Fluids A 3* (1991), 1760–1765.

[11] Germano, M., Piomelli, U., Moin, P., and Cabot, W. Erratum. *Phys. Fluids A 3* (1991), 3128.

[12] Ghosal, S., Lund, T., Moin, P., and Akselvoll., K. Corrigendum. *Journal of Fluid Mechanics 297* (1995), 402.

[13] Ghosal, S., Lund, T., Moin, P., and Akselvoll., K. A dynamic localization model for large-eddy simulation of turbulent flows. *Journal of Fluid Mechanics 286* (1995), 229–255.

[14] Karlsson, R., Eriksson, J., and Persson, J. LDV measurements in an plane wall jet in a large enclosure. In *Laser Techniques and Applications in Fluid Mechanics* (1993), D. D. o. R.J. Adrian, F. Durst, M. Heitor, M. Maeda, and J. H. J.H. Whitelaw, Eds., Springer-Verlag, pp. 311–332.

[15] Nielsen, P. Specification of a two-dimensional test case. Report, ISSN 0902-7513 R9040, Dept. of Building Technology and Structural Engineering, Aalborg Universitetscenter, Aalborg, 1990.

[16] Nilsson, H. A parallel multiblock extension to the CALC-BFC code using PVM. Rept. 97/11, Dept. of Thermo and Fluid Dynamics, Chalmers University of Technology, Gothenburg, 1997.

[17] Olsson, M. *Large Eddy Simulation of Turbulent Jets.* PhD thesis, Dep. of Mechanics, Royal Institute of Technology, Stockholm, 1997.

[18] Olsson, M., and Fuchs, L. Large eddy simulation of the proximal region of a spatially developing circular jet. *Phys. Fluids A 8* (1996), 2125–2137.

[19] Piomelli, U. High Reynolds number calculations using the dynamic subgrid-scale stress model. *Phys. Fluids A 5* (1993), 1484–1490.

[20] Piomelli, U., and Junhui, L. Large-eddy simulation of rotating channel flow using a localized dynamic model. *Phys. Fluids 7* (1995), 839–848.

[21] Restivo, A. *Turbulent Flow in Ventilated Rooms.* PhD thesis, University of London, Imperial College of Science and Technology, Mechanical Engineering Department, 1979.

[22] Voke, P., Gao, S., and Leslie, D. Large-eddy simulations of plane impinging jets. *Int. J. Numer. Meth. Engng. 38* (1995), 489–507.

[23] Yang, K.-S., and Ferziger, J. Large-eddy simulation of turbulent obstacle flow using a dynamic subgrid-scale model. *AIAA J. 31* (1993), 1406–1413.

[24] Zang, Y., Street, R., and Koseff, J. A dynamic mixed subgrid-scale model and its application to turbulent recirculating flows. *Phys. Fluids A 5* (1993), 3186–3196.

[1] available as postscript file at http://www.tfd.chalmers.se/~lada